Proton-decaying states in light nuclei and the first observation of ^{17}Na

K. W. Brown, R. J. Charity, J. M. Elson, W. Reviol, and L. G. Sobotka
Departments of Chemistry and Physics, Washington University, St. Louis, Missouri 63130, USA

W. W. Buhro, Z. Chajecki,* W. G. Lynch, J. Manfredi, R. Shane, R. H. Showalter, M. B. Tsang, D. Weisshaar, and J. R. Winkelbauer
National Superconducting Cyclotron Laboratory and Department of Physics and Astronomy, Michigan State University, East Lansing, Michigan 48824, USA

S. Bedoor†
Department of Physics, Western Michigan University, Kalamazoo, Michigan 49008, USA

A. H. Wuosmaa
Department of Physics, University of Connecticut, Storrs, Connecticut 06269, USA
and Department of Physics, Western Michigan University, Kalamazoo, Michigan 49008, USA

(Received 27 August 2016; revised manuscript received 28 February 2017; published 28 April 2017)

An upper limit to the mass of the three-proton unbound nucleus ^{17}Na was measured to be $\Delta M \leqslant 34.72(6)$ MeV. The excitation energies, widths, and decay modes for one- and two-proton decaying states of ^{8}B, ^{9}B, ^{9}C, ^{16}F, and ^{17}Ne were also measured. The energy-angular decay correlations in the $2p$ decay of ^{17}Ne are presented.

DOI: 10.1103/PhysRevC.95.044326

I. INTRODUCTION

Many ground and excited states of light, proton-rich nuclei decay by emitting one or more protons. The excitation energy and intrinsic width of these proton decaying states can be accessed via the invariant mass of the detected decay fragments. With the apparatus used for the present work, this continuum-spectroscopy technique has been used to study the ground and excited states of ^{16}Ne [1,2] and the isobaric analog state in ^{8}B [3]. For two-proton decaying states, this method can also determine whether the decay occurs directly or by two sequential one-proton decays through an intermediate nucleus by measuring the energy and angular correlations between the decay fragments. In this paper we present new information on the excited states of the proton-rich nuclei ^{8}B, ^{9}B, ^{9}C, ^{16}F, and ^{17}Ne, and the first observation of the proton unbound nucleus ^{17}Na.

II. EXPERIMENTAL METHOD

This work made use of two secondary beams produced by the Coupled Cyclotron Facility at the National Superconducting Cyclotron Laboratory at Michigan State University: ^{9}C ($E/A = 68$ MeV, intensity $= 5.0 \times 10^{4}$ pps, 52% purity) produced from a ^{16}O primary beam ($E/A = 150$ MeV, 175 p nA) and ^{17}Ne ($E/A = 58$ MeV, intensity $= 1.6 \times 10^{4}$ pps, 11% purity, where the largest component of the total intensity of 1.5×10^{5} was ^{15}O) from a ^{20}Ne primary beam ($E/A =$ 170 MeV, 80 p nA). The details of these experiments have been published elsewhere [1,3]. In brief, these secondary beams bombarded a 1-mm-thick ^{9}Be target. Reactions on ^{9}Be target nuclei produced short-lived states, which decayed within the target. Charged particles from those decays were detected in the High Resolution Array (HiRA) [4]. In these experiments the HiRA array comprised 14 Si-CsI(Tl) telescopes, centered around the beam in vertical towers in a 2-3-4-3-2 arrangement. The middle tower had a 1.44-inch-tall gap in the middle to allow the unreacted beam to pass through. The silicon part of a telescope was a 1.5-mm-thick double-sided strip detector consisting of 32-strip segments in orthogonal directions and covering an active area of 64×64 mm^2. Each silicon detector was backed by four 4-cm-thick CsI(Tl) scintillators, each of the four spanning a quadrant of the preceding silicon.

The γ-ray array CAESAR (CAESium iodide ARray) surrounded the target to detect any γ rays in coincidence with the charged particles emitted in the decays [5]. For these experiments the array consisted of 158 CsI(Na) crystals covering the polar angles between 57.5° and 142.4° in the laboratory, with complete azimuthal coverage. The first ring and the last two rings of the full CAESAR array were removed due to space constraints.

III. RESULTS

Table I contains the deduced properties of the levels measured in this work, including the centroids, intrinsic widths, and decay modes. The rest of this section presents more detailed discussions of each case. The excitation energies were determined via the invariant-mass method, in which the total kinetic energy of the fragments is measured and the deduced center-of-mass decay energy E_T is corrected for the decay Q value. The reconstructed excitation-energy resolution was determined from Monte Carlo simulations that take into

*Present address: Department of Physics, Western Michigan University, Kalamazoo, Michigan 49008, USA.
†Present address: Cyclotron Institute, Texas A&M University, College Station, Texas 77843, USA.

TABLE I. A summary of the excitation energies, intrinsic widths, spins, parities, isospin, and decay modes of the states for which new information was measured. For ground-state decays, the decay energy is quoted in addition to the excitation energy.

Nucleus	E^* (MeV)	Γ (keV)	J^π	T	Decay mode	Branching ratio
^{8}B	0.7695(25)[a]	35.6(6)[a]	1^+[a]	1	$p + {}^{7}\mathrm{Be}_{g.s}$	$98.9 \pm 1.8\%$
				1	$p + {}^{7}\mathrm{Be}_{1/2^-}$	$1.1 \pm 0.3\%$
^{8}B	2.320(20)[a]	350(30)[a]	3^+[a]	1	$p + {}^{7}\mathrm{Be}_{g.s.}$	
^{9}B	19.254(23)	1370(800)	$(1/2^+, 5/2^+)$	(3/2)	$p + {}^{8}\mathrm{Be}_{1^+}$	
^{9}B	19.694(12)	590(290)		(1/2)	$p + {}^{8}\mathrm{Be}_{1^+}$	
^{9}B	20.423(33)	440(80)		(3/2)	$p + {}^{8}\mathrm{Be}_{3^+}$	
^{9}C	2.218(11)[a]	52(11)	$1/2^-$[a]	3/2	$p + {}^{8}\mathrm{B}_{g.s.}$	
^{9}C	3.549(20)	673(50)	$5/2^-$[a]	3/2	$p + {}^{8}\mathrm{B}_{g.s.}$	
^{9}C	4.40(4)	2750(110)	$(1/2^+, 5/2^+)$	3/2	$p + {}^{8}\mathrm{B}_{1^+}$	
^{9}C	5.75(4)	601(50)		3/2	$p + {}^{8}\mathrm{B}_{3^+}$	
^{16}F	7.67(4)			(1)	$2p + {}^{14}\mathrm{N}$	
^{16}F	10.26(4)			(1)	$2p + {}^{14}\mathrm{N}$	
^{17}Ne	1.764(12)[a]		$5/2^-$[a]	3/2	$p + {}^{16}\mathrm{F}_{g.s.}$	
^{17}Na	0.0 [$E_T \leqslant 4.85(6)$]		$(1/2^+)$	3/2	$3p + {}^{14}\mathrm{O}$	

[a]Value from tabulation [6].

account effects of detector resolution, geometrical efficiency, and energy loss and small-angle scattering in the target [1]. The CsI(Tl) detector resolution was adjusted in the simulation to reproduce the widths of low-lying, narrow resonances in ^{6}Li, ^{9}B, and ^{17}Ne.

A. ^{17}Na

States in ^{17}Na can be populated with a ^{17}Ne beam either by charge-exchange reactions with the target or through more complicated reactions. Prior to this work it was known that ^{17}Na was unbound, but its continuum structure was unexplored. The decay-energy spectrum for $^{17}\mathrm{Na} \rightarrow 3p + {}^{14}\mathrm{O}$ is shown in Fig. 1. There is a peak in the spectrum located at $E_T = 4.85(6)$ MeV that sits on top of a background. This background has contributions from ^{15}O nuclei which are misidentified as ^{14}O and can be accurately modeled by taking detected $3p + {}^{15}\mathrm{O}$ events and analyzing them as $3p + {}^{14}\mathrm{O}$ events. The resulting spectrum is shown as the red dashed line in Fig. 1, where the amount of leakage is based on that observed for the $^{16}\mathrm{Ne} \rightarrow 2p + {}^{14}\mathrm{O}$ events from $2p + {}^{15}\mathrm{O}$ events in Ref. [1]. No narrow resonances in the $3p + {}^{15}\mathrm{O}$ channel were populated, so the resulting background is featureless. To ensure that the observed decays are coming from ^{17}Na and not from random coincidences, we have reconstructed the excitation energy of the ^{9}Li target remnant, the spectrum of which is shown in Fig. 2. Results are shown for a gate around the ~5 MeV peak. Yield for $E^*_{\mathrm{target}} < 0$ MeV is unphysical and indeed most of the observed yield occurs at positive energies. The low-energy tail extending to negative energies can be accounted for by the simulated resolution of ~50 MeV (FWHM). Thus this spectrum is consistent with a physical process.

The mirror nucleus, ^{17}C, has a $J^\pi = 3/2^+$ ground state, and $1/2^+$ and $5/2^+$ excited states at 210 and 331 keV respectively [13]. For a $3p$ decay at 4.85 MeV, Monte Carlo simulations predict a full width at half maximum (FWHM) of

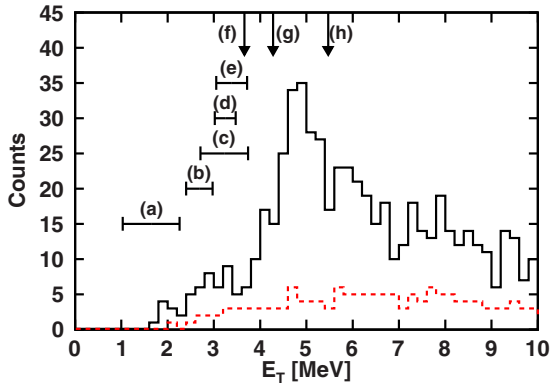

FIG. 1. Decay-energy spectrum of ^{17}Na from all detected $3p + {}^{14}\mathrm{O}$ events. The red dashed histogram corresponds to $3p + {}^{15}\mathrm{O}$ events which have been analyzed as $3p + {}^{14}\mathrm{O}$ events. The labeled horizontal bars correspond to the range of predicted energies for the first three states in ^{17}Na reported in (a) [7], (b) [8], (c) [9], (d) [10], and (e) [9]. The labeled solid arrows indicate the ground-state mass predicted by systematics reported in (f) [11], (g) [11], and (h) [12].

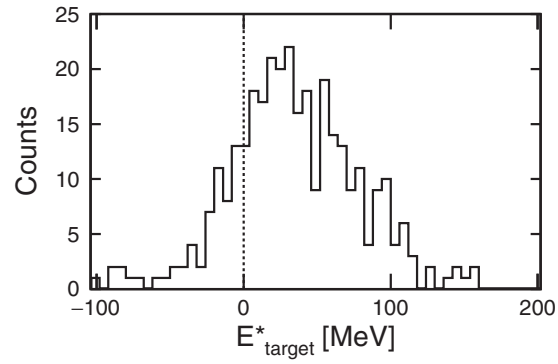

FIG. 2. Reconstructed target excitation-energy spectrum gated on the ^{17}Na decay energies between 4 and 6.5 MeV.

TABLE II. Theoretical predictions, sorted by decay energy, of the J^π and decay energy for the ground-state of ^{17}Na.

	Decay energy (MeV)	J^π	Reference
(a)	1.03	$1/2^+$	[7]
(b)	2.40	$1/2^+$	[8]
(c)	2.71	$1/2^+$	[9]
(d)	3.02	$1/2^+$	[10]
(e)	3.05	$1/2^+$	[9]
(f)	3.66	$3/2^{+b}$	[11]
(g)	4.28	$3/2^{+b}$	[11]
(h)	5.47[a]	$3/2^{+b}$	[12]

[a]The masses presented in Ref. [12] are used to calculate the decay energy (their presented separation energies are inconsistent with their masses).
[b]Obtained from mass systematics and so assume the same ground-state spin as for the mirror.

the reconstructed energy to be 540 keV, accounting for device resolution and acceptance. The FWHM of the detected peak is 1150 keV. Therefore this peak is either a wide state or some mixture of all three of these states. A fit assuming a single peak yields $E_T = 4.85(6)$ MeV.

If this peak is a mixture of levels or even a highly-lying excited state, then its energy gives an upper limit for the mass excess of ^{17}Na, $\Delta M(^{17}\text{Na}) \leqslant 34.72(6)$ MeV. Table II has a list of the different theoretical predictions for the ground-state decay energy. The predictions vary widely between $E_T = 1.03$ and 5.47 MeV. Our upper limit on the mass only rules out the prediction from systematics in Ref [12]. The labeled horizontal bars in Fig. 1 indicate the predicted energy ranges for the first three states ($1/2^+$, $3/2^+$, and $5/2^+$) for the models listed in Table II. If our observed peak is from the decay of one or more of these levels, the location of this peak is inconsistent with the model predictions of Refs. [7–10]. Thus either these models are incorrect or the observed peak corresponds to higher-lying excited state(s). Indeed there is some yield above background below this peak at $E_T \sim 3$ MeV which would be consistent with yield from the ground-state triplet in models [8–10]. The closest prediction to our peak is the upper value from Ref [11] obtained from the Kelson and Garvey formula. The models that predict the J^π of the ground state agree that it is $1/2^+$. Shell-model calculations suggest that the $1/2^+$ state has two of the valence $d_{5/2}$ nucleons coupled to 0^+ and the third valence nucleon in the second $s_{1/2}$ orbit [14]. The third valence proton is in the $s_{1/2}$ orbit which leads to a Thomas-Ehrman shift, potentially lowering its energy relative to the ground state of ^{17}C.

B. ^{9}C

Excited states of ^{9}C were populated through inelastic scattering of the ^{9}C beam with the ^{9}Be target. A partial level scheme for the one- and two-proton decays of ^{9}C is shown in Fig. 3. Previously known information (energy, spin-parity, width, and decay modes) is plotted in black for ^{9}C and the low-lying states in the daughter nuclei. The ground state is the only particle-bound state in ^{9}C, with the first-excited state

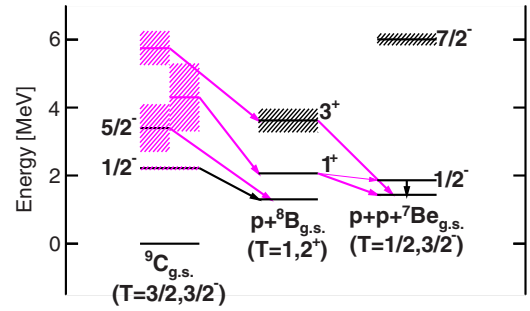

FIG. 3. Partial level scheme for the proton decay of ^{9}C and ^{8}B. Levels are labeled by their spin and parity (J^π) when known. New levels, widths, or decay modes are plotted in magenta.

more than 1 MeV above the proton-decay threshold. The invariant-mass spectrum of ^{9}C from all detected $p + ^8$B events is displayed in Fig. 4. The two prominent peaks correspond to the known first- and second-excited states with $J^\pi = 1/2^-$ and $5/2^-$, respectively. Both states decay by one-proton emission to the $J^\pi = 2^+$ ground state of ^{8}B.

To extract the level energy and width for each of these states, the invariant-mass spectrum was fit using R-matrix line shapes [15]. The red solid curve in Fig. 4 is the best fit with the excitation energy for the first-excited state fixed at the known value (2.218(11) MeV [6]) and the energy for the second-excited state extracted from the fit. The fit includes the individual R-matrix simulations of each peak (blue dashed and green dotted lines respectively) as well as a smooth background (orange dot-dashed line). The line shapes of the individual peaks are taken from the R-matrix prescription and incorporated into Monte Carlo simulations to account for detector resolution and acceptance. The background is of unknown origin, and several different parametrizations of the background were explored. The effect of the choice of background on the centroid and width of the measured states is folded into the listed uncertainty. The amplitudes of the line shapes and the parameters for the background were then simultaneously fit for each decay energy and width pair to extract the overall best fit to the data. The width

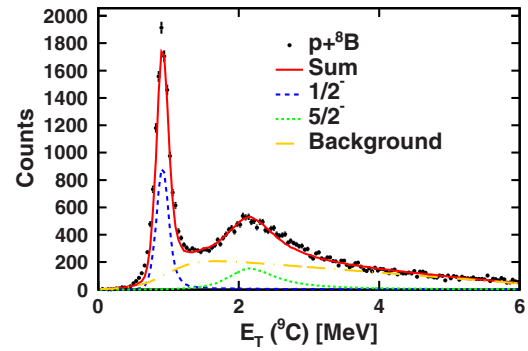

FIG. 4. Invariant-mass spectrum of ^{9}C from all detected $p + ^8$B events. The blue dashed and green dotted lines are R-matrix simulations for the $1/2^-$ and $5/2^-$ states; each curve has been scaled down by a factor of 2 for clarity. The orange dot-dashed line is one parametrization of the background considered. The sum of the background and two simulations is plotted as the red solid line.

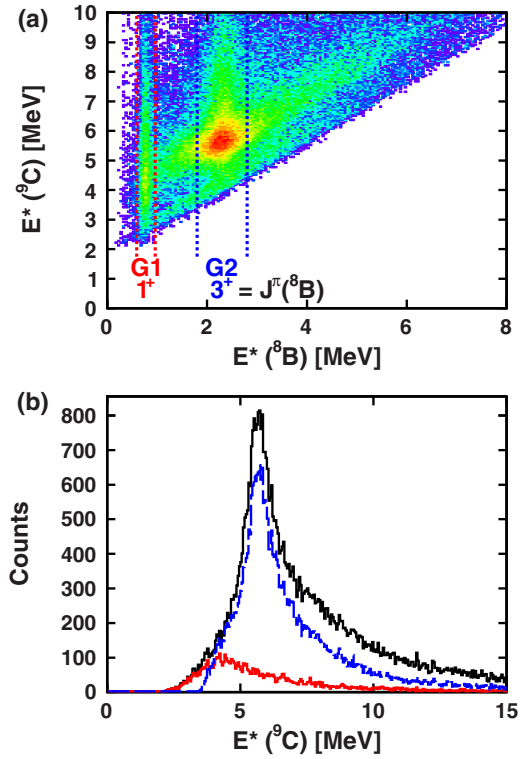

FIG. 5. (a) Excitation-energy spectrum for $2p + {}^7$Be events plotted as a function of the excitation energy for the intermediate state (^{8}B) for each $p + {}^7$Be combination. (b) Excitation-energy spectrum for ^{9}C from all detected $2p + {}^7$Be events (black). The red and blue histograms are the spectra for events with ^{8}B excitation energy falling in gates G1 and G2, respectively.

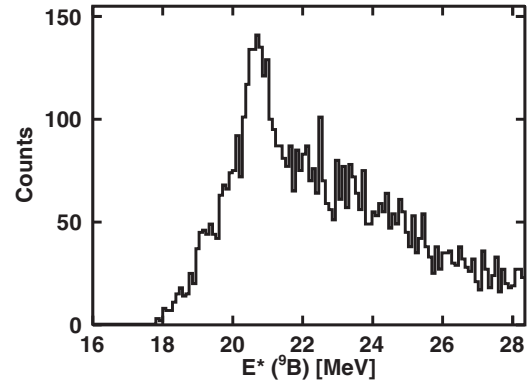

FIG. 6. Excitation-energy spectrum of ^{9}B from all $p + p + {}^7$Li events.

extracted for the first-excited state is $\Gamma = 52 \pm 11$ keV. The excitation energy of the second-excited state was found to be $E^* = 3.549 \pm 0.020$, with a width of $\Gamma = 673 \pm 50$ keV. The extracted width of the first-excited state is much lower than the value of $\Gamma = 100 \pm 20$ keV obtained from (^{3}He,^{6}He) transfer in Ref. [16]. Recent *ab initio* calculations with the variational Monte Carlo method predict the width to be $\Gamma = 102 \pm 5$ keV [17], which is consistent with the transfer work, but inconsistent with our measurement. However, even more recent results from the shell model with the source-term approach (STA) predict a width of $\Gamma_{\rm STA} = 53$ keV, which reproduces our result [18]. The standard approach to the shell model also agrees with our result, $\Gamma_{\rm SM} = 58.7$ keV [18].

At $E^* = 1.436(18)$ MeV, ^{9}C becomes unbound with respect to two-proton emission. The black histogram in Fig. 5(b) shows the invariant-mass spectrum from all detected $2p + {}^7$Be events. A wide, asymmetric peak at around 5.5 MeV can be seen. These ^{9}C excited states can decay sequentially through proton-unbound excited states of ^{8}B. To search for these intermediate states, we reconstruct the excitation energy of the ^{8}B intermediate state. As we cannot determine which of the two protons came from the decay of a ^{8}B intermediate state, we calculate two ^{8}B excitation energies from the invariant mass of each of the protons in coincidence with ^{7}Be; see Fig. 5(a). Two peaks can be seen, corresponding to the $J^\pi = 1^+$ and 3^+ excited states in ^{8}B. Gating on these two states, indicated by the regions labeled G1 and G2 in Fig. 5(a), reveals two different peaks from the ^{9}C invariant-mass spectrum, see Fig. 5(b). The G1 gate (red histogram) corresponds to a state in ^{9}C at 4.40 (4) MeV, decaying through the 1^+ state in ^{8}B, and the G2 gate (blue histogram) is associated with a state at 5.75 (4) MeV, decaying through the 3^+ state. We fit each of these peaks using an R-matrix line shape with a smooth background, and determine the widths to be $\Gamma = 2.75 \pm 0.11$ MeV and $\Gamma = 601 \pm 50$ keV, respectively. The 4.40 MeV state was seen previously from (^{3}He,^{6}He) transfer reactions, although only the excitation energy was reported (4.3 MeV) [19].

C. ^{9}B

The ground state and low-lying excited states of ^{9}B decay into the $p + \alpha + \alpha$ exit channel. The invariant mass from this exit channel was published previously in Ref. [20]. In the same paper, the $2p + {}^7$Li spectrum was also analyzed. Due to saturation in the silicon amplifiers, only a small fraction of ^{7}Li fragments were identified. In the current experiment this saturation problem was fixed, and we have the full range of ^{7}Li fragments. The ungated excitation-energy spectrum for all $2p + {}^7$Li events is shown in Fig. 6. A peak around 20 MeV can be seen on top of a large background. This peak is above both the $1p$ and $2p$ decay thresholds. As we did for the $2p$ decay of ^{9}C (see Sec. III B), we can reconstruct the excitation energy of the $1p$ intermediate, in this case ^{8}Be. If this state in ^{9}B decays sequentially through one of the excited states of ^{8}Be, we can gate our events on the energy of this intermediate to remove some background. Figure 7(a) shows the excitation energy of ^{9}B as a function of the excitation energy of the ^{8}Be intermediate. We reconstruct the excitation energy of the ^{8}Be for each of the $p + {}^7$Li possibilities. In Fig. 7(a) one can see that the decay of ^{9}B has yield proceeding through three different ^{8}Be excited states. Gating on each of these intermediate states isolates three different states in ^{9}B.

Figure 7(b) shows the $2p + {}^7$Li spectrum where one of the two $p + {}^7$Li combinations correctly reconstructs the $E^* = 17.640(1)$ MeV, $J^\pi = 1^+$, $T = 1$ ^{8}Be intermediate state (gate G1). This intermediate state is likely the isobaric analog of the ^{8}B first-excited state. Following this logic, the state in ^{9}B isolated by the gate G1 is likely the analog of the $T = 3/2$

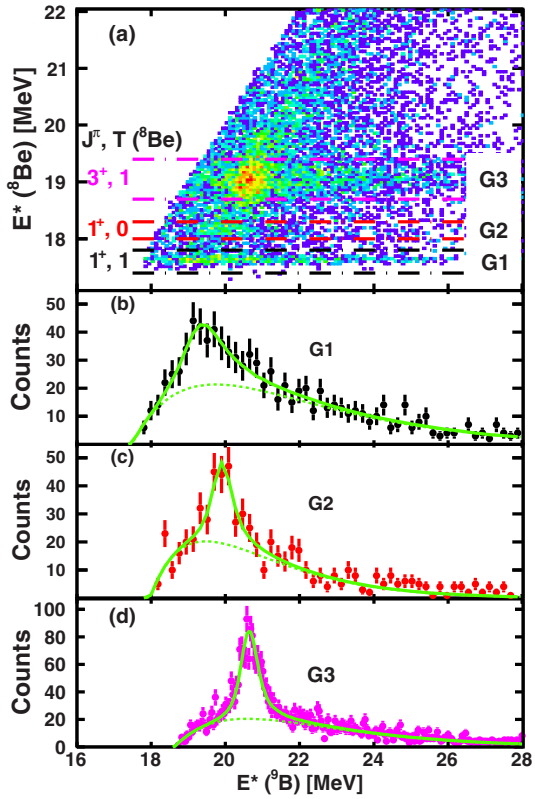

FIG. 7. (a) Excitation energy of ^{9}B as a function of the excitation energy of the ^{8}Be intermediate for all $p+p+^7$Li events. (b) Excitation energy of ^{9}B gated on the $J^\pi = 1^+, T = 1$ excited state in ^{8}Be (gate G1). (c) Excitation energy of ^{9}B gated on the $J^\pi = 1^+, T = 0$ excited state in ^{8}Be (gate G2). (d) Excitation energy of ^{9}B gated on the $J^\pi = 3^+, T = 1$ excited state in ^{8}Be (gate G3). Each spectrum in panels (b)–(d) has been fit using the R matrix and a smooth background. The fits are the solid lines and the background contributions are the dashed lines.

state in ^{9}C at $E^* = 4.4$ MeV; see Sec. III B. A fit of this resonance can be seen in Fig. 7(b) as the solid line. The line shape used for this fit was taken from the R matrix as in previous sections and a smooth curve was chosen to reproduce the background (dashed line). The excitation energy extracted from the fit is $E^* = 19.254(23)$ MeV with an intrinsic width of $\Gamma = 1.37(80)$ MeV.

The gate G2 selects $2p+^7$Li events that decay through the $E^* = 18.150(4)$ MeV, $J^\pi = 1^+, T = 0$ ^{8}Be intermediate state. The $2p$ decaying state in ^{9}B is therefore likely a $T = 1/2$ excited state. A similar R-matrix analysis was performed as for the state associated with G1, and the extracted energy and width were $E^* = 19.694(12)$ MeV and $\Gamma = 590(290)$ keV.

The final gate G3 corresponds to the $E^* = 19.069(10)$, $J^\pi = 3^+, T = 1$ ^{8}Be intermediate state, which is the analog of the ^{8}B second excited state. In Ref. [20] they reported a $2p$ decaying state in ^{9}B that decayed through this ^{8}Be intermediate at $E^* = 20.64(10)$ MeV and $\Gamma = 450(250)$ keV. A fit of this resonance yields an excitation energy of $E^* = 20.423(33)$ MeV and $\Gamma = 440(80)$ keV, which consistent with that measurement. This state is likely the $T = 3/2$ analog of the $E^* = 5.75(4)$ MeV state seen in ^{9}C in Sec. III B.

D. $A = 9$ analog states

If the 19.254 and 20.423 MeV states in ^{9}B are analogs of the 4.40 and 5.75 MeV states in ^{9}C, then they should have consistent Coulomb-displacement energies (ΔE_C) to those associated with the lower-lying ^{9}C states.

Using the masses and excitation energies from Refs. [6,21], we calculate Coulomb-displacement energies of 2.621(3) and 2.418(12) MeV for the ground state ($J^\pi = 3/2^-$) and the first-excited state ($J^\pi = 1/2^-$) of ^{9}C, respectively. For the $^9C_{5.75}$–$^9B_{20.423}$ pair, our fitted energies give $\Delta E_C = 2.60(51)$ MeV which is consistent within the error to the ground-state value. Now for the $^9C_{4.40}$–$^9B_{19.254}$ pair we obtain $\Delta E_C = 2.422(46)$ MeV, about 200 keV lower in energy but similar to the value for the first-excited state. The consistency of these values further supports our contention that these are analog states.

Smaller values of the Coulomb displacement energy are associated with more extended proton configurations. For example, proton strength in a valence $s_{1/2}$ orbital produces a Thomas-Ehrman shift [22] decreasing ΔE_C. While this physics is not applicable to the first excited state of ^{9}C, it is worth considering the possibilities for the $^9C_{4.40}$–$^9B_{19.254}$ pair where the emission of a $s_{1/2}$ proton could also explain the large widths of these states.

Putting proton strength in the second $s_{1/2}$ orbit creates positive-parity states. At present no such levels are known in ^{9}C or its mirror ^{9}Li. Indeed, the location of the lowest-lying positive-parity states in ^{9}C and ^{9}Li are of interest in explaining the anomalous magnetic moment of the ^{9}C ground state [23]. Due to the Thomas-Ehrman effect there may be more mixing with intruder configurations in the ^{9}C ground state compared to the mirror ^{9}Li state.

Using the R-matrix prescription [15] and calculating the dimensionless reduced width θ^2 from the wave function calculated with a Coulomb plus Wood-Saxon nuclear potential of diffuseness $a = 0.65$ fm, radius parameter $r_0 = 1.25$ fm, and depth adjusted to get the decay energy correct, we find the widths for $\ell = 0,1,2$ decays are $\Gamma = 5.3$, 1.7, and 0.6 MeV respectively, assuming a spectroscopic factor of unity. The experimental value for ^{9}C is 2.750(11), consistent with the emission of an $s_{1/2}$ proton with an spectroscopic factor of 0.52, while a large value of 1.6 is required for $\ell = 1$ decay.

To investigate plausible spectroscopic strengths, we have performed shell-model calculations with the OXBASH code [24] using the *psd* shell and the *psd* WBP interaction [25]. For the lowest $J^\pi = 1/2^+$ states, the spectroscopic factor for this $s_{1/2}$ decay was calculated as 0.28, a little lower than the value needed to reproduce the experimental width. On the other, no other low-lying states were calculated as having very large $\ell = 1$ spectroscopic strength to the $J^\pi = 1^+$ ^{8}B level. Thus within the shell model, $J^\pi = 1/2^+$ is the only possible assignment for this level. However, s-wave emission to a $J^\pi = 1^+$ level can also be associated with a $J^\pi = 5/2^+$ state.

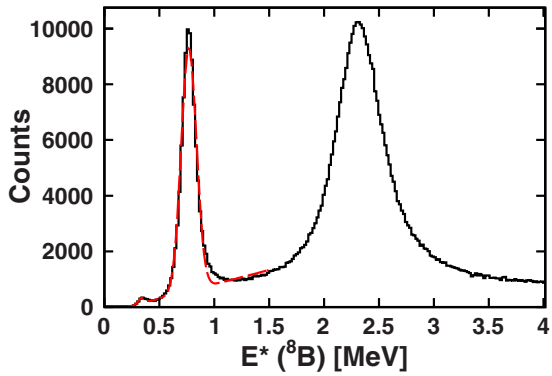

FIG. 8. Excitation-energy spectrum of ^{8}B from all $p + ^7$Be events (black solid line). The two lower-energy peaks produced by decay of the 1^+ state are fit with the sum of two Gaussians and a linear background (dashed line).

E. ^{8}B

The two-proton decay of ^{8}B was studied recently [3], and the one-proton decay to high-lying excited states of ^{7}Be that decay to ^{3}He + α was discussed in Ref. [20]. Here we discuss one-proton decay to the particle-bound states of ^{7}Be. A partial level scheme for ^{8}B appears in Fig. 3. The energy and width of the first two excited states in ^{8}B have been known for a long time [6]; however, their decay modes had not been studied directly. The 1^+ and 3^+ levels are both unbound with respect to proton decay to the ground state ($3/2^-$) and first-excited state ($1/2^-$) of ^{7}Be. The first-excited state of ^{7}Be decays via emission of a 429 keV γ ray to the ground state. The invariant-mass spectrum for ^{8}B from all $p + ^7$Be events is shown in Fig. 8. The two prominent peaks at $E^* = 0.7695(25)$ and 2.320(20) MeV correspond to the first two excited states of ^{8}B. A tiny peak at 0.340 MeV arises from events where the first-excited state in ^{8}B is populated and decays to the first-excited state of ^{7}Be. As the γ-ray energy is not included in the invariant mass, this branch appears at a lower apparent excitation energy. Figure 9 shows the γ-ray energy spectrum gated on this small peak. This spectrum is Doppler corrected and has add-back from neighboring crystals. The blue dashed line corresponds to one estimation of the beam-correlated background, which was generated by gating on events in the $^9\mathrm{B} \rightarrow p + 2\alpha$ channel, which has no bound, excited states that produce γ rays. The detection thresholds for most crystals were between 200 and 300 keV. The expected 429-keV γ ray is clearly observed.

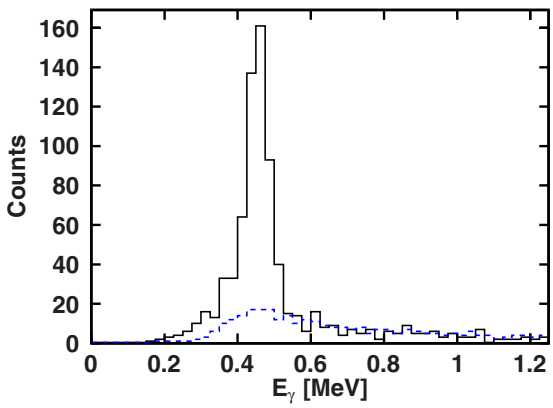

FIG. 9. The black solid histogram is the γ-ray energy spectrum gated on the tiny peak in the ^{8}B invariant-mass spectrum at $E^* = 0.34$ MeV. The spectrum has been Doppler corrected ($\beta = 0.362$) and has add-back from neighboring crystals. The blue dashed histogram is a CAESAR γ-ray background.

We can extract a branching ratio for the decay of the 1^+ state to either the $3/2^-$ ground state or $1/2^-$ first-excited state in ^{7}Be. By fitting both peaks in the excitation-energy spectrum and extracting the areas (with uncertainties dominated by background contributions), and correcting for the detector efficiency (20.5% and 24.9% respectively), the branching ratio was found to be $1.1 \pm 0.3\%$ to the $1/2^+$ excited state and $98.9 \pm 1.8\%$ to the $3/2^+$ ground state of ^{7}Be. The partial proton width for decay to the ground state was measured in proton scattering on ^{7}Be [26], with a value of $\Gamma_p = 0.026(6)$ MeV. Comparing this to the total width, $\Gamma_{tot} = 0.027(6)$ MeV, yields a branching ratio to the ground state of $96 \pm 30\%$, in agreement with the present result but with much larger uncertainty.

F. ^{16}F

1. Background

In Ref. [3] evidence for a new type of direct $2p$ decay was presented between two isobaric-analog states (IAS). The daughter nucleus then deexcites to its ground state via γ-ray emission. The $^8\mathrm{B}_{\mathrm{IAS}}$ was the first case for this decay mode where all of the decay products were measured (two protons, the ^{6}Li core, and the γ). Another possible case was observed in the $2p + ^{10}$B decay channel corresponding to a state in ^{12}N [27]. If the ^{10}B nucleus were formed in its ground state, then the measured excitation energy of this peak would not correspond to any known state in either ^{12}N or its mirror ^{12}B. However, $^{12}\mathrm{N}_{\mathrm{IAS}}$ should decay to $^{10}\mathrm{B}_{\mathrm{IAS}}$, in a way analogous to the decay of $^8\mathrm{B}_{\mathrm{IAS}}$. The $^{10}\mathrm{B}_{\mathrm{IAS}}$ is known to decay via γ emission, but the γ rays were not measured in that experiment. However, adding in this missing energy from the γ ray brings the measured energy to the predicted excitation energy of $^{12}\mathrm{N}_{\mathrm{IAS}}$ from the isobaric mass multiplet equation (IMME). Thus while this decay mode was not confirmed in this case (no γ ray measured), the measurement of the decay mode of $^8\mathrm{B}_{\mathrm{IAS}}$ lends strong support to the IAS-to-IAS $2p$ decay route.

Moving higher in mass, the next isobaric analog state that could decay in this manner is $^{16}\mathrm{F}_{\mathrm{IAS}}$. While this resonance has never been observed, its energy can be predicted from the IMME for $A = 16$. The residuals of a quadratic fit of the known $A = 16$ masses are shown in Fig. 10. The quadratic fit of the $A = 16$, $T = 2$ quintet contains the new mass for $^{16}\mathrm{Ne}_{g.s.}$ from Ref [1] and takes the other masses from the most recent mass evaluation [21]. This fit predicts an excitation energy for $^{16}\mathrm{F}_{\mathrm{IAS}}$ of 10.116 (6) MeV, which is displayed as the green level in the partial level scheme shown in Fig. 11. As was true in both $^8\mathrm{B}_{\mathrm{IAS}}$ and $^{12}\mathrm{N}_{\mathrm{IAS}}$, the only isospin- and energy-allowed particle decay mode is a $2p$ emission to the isobaric analog state of the daughter state in ^{14}N. The $^{14}\mathrm{N}_{\mathrm{IAS}}$ decays by emission of a 2.313 MeV γ ray to the ground state. If this $2p$ decay were to be observed in an invariant-mass spectrum, the peak would be located at ~7.8 MeV.

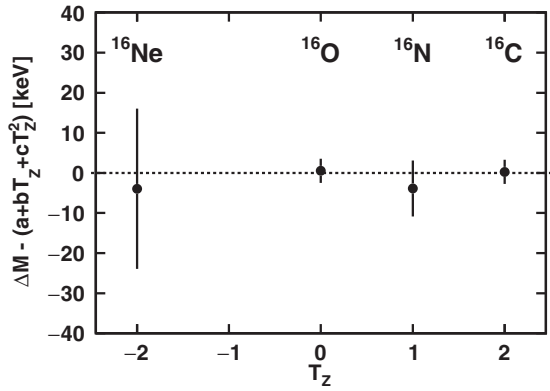

FIG. 10. Deviation from the fitted quadratic form of the IMME for the lowest $T = 2$ states in the $A = 16$ isobar.

2. Two-proton decay

With a ^{17}Ne beam, $T = 2$ ^{16}F states can be populated in proton-knockout reactions. If $^{16}F_{IAS}$ is populated, one expects to see a peak at the position of the red arrow in the $2p + ^{14}$N invariant mass spectrum, which is shown in Fig. 12(a). There is a small peak observed in this region (see inset) but it is approximately 200 keV lower than the expected position of the IAS. While this does not rule out the possibility that it is the IAS, it is highly unusual for the energy of an analog state to deviate that much from the quadratic form of the IMME. Furthermore, if this were the IAS, it must be in coincidence with the 2.313 MeV γ ray from the decay of $^{14}N_{IAS}$. The energy spectrum of γ rays in coincidence with events in the region of the observed peak are shown in Fig. 12(b). For a 2.3 MeV γ ray, the photopeak efficiency of CAESAR is ~20%; i.e., with roughly 100 events in the peak we should measure 20 events in the photopeak, which is clearly not consistent with this spectrum. While higher statistics are required to completely rule out the IAS-to-IAS decay path, our data strongly suggest that the observed peak corresponds to a $T = 1$ state at $E^* = 7.67 \pm 0.04$ MeV. This is likely the analog of the $E^* = 7.674$ MeV state in the mirror, ^{16}N, for which no J^π assignment was made.

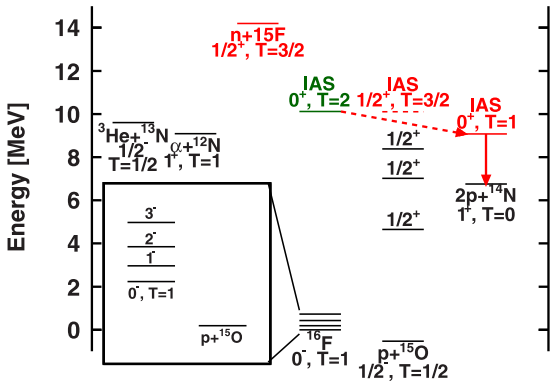

FIG. 11. Partial level scheme for the decay of $^{16}F_{IAS}$ (level in green). Colored levels indicate isospin-allowed decays from the $^{16}F_{IAS}$. All energies are relative to the ground state of ^{16}F. The inset shows an expanded level scheme for the low-lying states of ^{16}F.

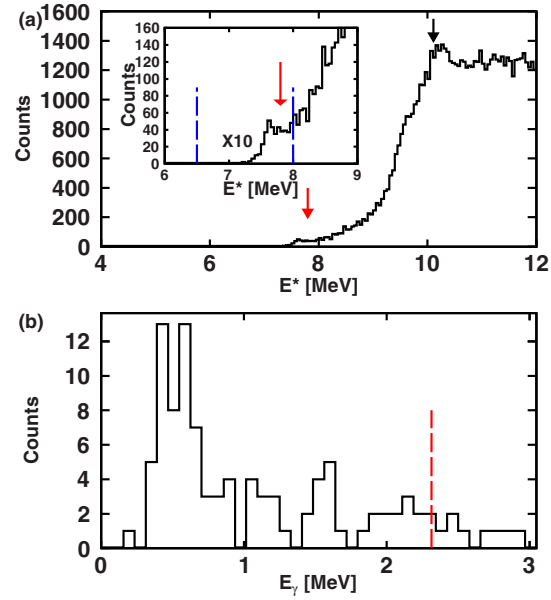

FIG. 12. (a) Excitation-energy spectrum of ^{16}F from all detected $2p + ^{14}$N events. The inset shows the same histogram expanded in the region around the expected $^{16}F_{IAS}$ peak. (b) γ-ray-energy spectrum measured in coincidence with events inside of the gate indicated in (a) with the blue dashed lines. The expected photopeak position (2.313 MeV) is marked with the red dashed line.

The decay energies for the IAS-to-IAS transitions are listed in Table III for this and the other two cases we have studied. For higher Z nuclei the decay energy becomes smaller and the Coulomb barrier becomes larger. Given the two protons are emitted simultaneously, the decay width should be proportional to the product of their barrier penetration factors, which is maximized for when the two proton energies are equal. Thus the contribution from the barrier penetration should go roughly as the square of the single-proton penetration factor at $E_T/2$. Such P_ℓ values are listed in Table III. For $^{16}F_{IAS}$ (in the sd shell), if the $2p$ decay involves the emission of two $d_{5/2}$ protons, then $(P_\ell)^2$ is smaller by a factor of ~10^5 from

TABLE III. Decay energies (E_T) and barrier penetration factors (P_ℓ) for the decay channels relevant to this work. As ^{8}B and ^{12}N are p-shell nuclei, their penetration factors are calculated for $\ell = 1$. On the other hand ^{16}F is in the sd shell, so values are calculated for $\ell = 0,2$. The barrier penetration factors for $2p$ decays are calculated assuming that each proton takes away 1/2 E_T. Isospin-nonconserving decays are listed in the lower section of the table. A channel radius parameter of 1.45 fm was used to obtain these values.

Decay channel	E_T (MeV)	ℓ	P_ℓ
$^8B_{IAS} \rightarrow 2p + ^6Li_{IAS}$	1.312	1	0.0768
$^{12}N_{IAS} \rightarrow 2p + ^{10}B_{IAS}$	1.165	1	0.0177
$^{16}F_{IAS} \rightarrow 2p + ^{14}N_{IAS}$	1.046	0	0.0129
$^{16}F_{IAS} \rightarrow 2p + ^{14}N_{IAS}$	1.046	2	0.000141
$^{16}F_{IAS} \rightarrow 2p + ^{14}N_{g.s.}$	3.359	0	0.514
$^{16}F_{IAS} \rightarrow \alpha + ^{12}N_{g.s.}$	1.037	2	0.000034
$^{16}F_{IAS} \rightarrow ^3He + ^{13}N_{g.s.}$	0.523	1	7.0×10^{-8}

the $^{8}B_{IAS}$ case. However, for the emission of two $s_{1/2}$ protons there is still a suppression, but of much smaller magnitude ($\sim$10). The absence of the isospin-allowed $2p$ channel might be an indication that there is little $(1s_{1/2})^2$ proton strength for $^{16}F_{IAS}$. The suppression of the isospin-allowed $2p$ channel in $^{16}F_{IAS}$ will allow isospin-nonconserving channels to be more competitive.

3. *Isospin-nonconserving decays*

From phase-space considerations, one of the most competitive isospin-nonconserving decay mode for $^{16}F_{IAS}$ is $2p$ emission to the ground state of ^{14}N either directly or sequentially through an unbound, excited state of ^{15}O. If the energy predicted from the IMME is correct, then either possibility would produce a peak at the location of the black arrow in Fig. 12(a). While there is a peak near that energy in the $2p + {}^{14}N$ invariant mass spectrum, the excitation energy is $E^* = 10.26 \pm 0.04$ MeV, which is more than 100 keV more than the predicted energy. Deviations from the quadratic IMME are generally much smaller than this; however, a deviation of this magnitude was observed for the $A = 8$ quintet [28]. So although this may be the IAS, it also could be a previously unknown $T = 1$ state. Therefore, without further evidence that this is a $T = 2$ state, we conclude that it is probably a previously unknown $T = 1$ state. As the two peaks are suggestive of, but each inconsistent with, a pure $T = 2$ state, they may represent a mixed $T = 1,2$ $(J^\pi = 0^+)$ doublet. However, even in this case, the lack of evidence for a γ ray in coincidence with the structure seen at lower E_T is problematic.

Other possible energy-allowed but isospin-forbidden transitions are alpha emission and ^{3}He emission. Both decays have decay energies at or below 1 MeV and have angular momentum barriers. The barrier penetration factors are very small, and we do not see any yield to these channels. We also did not see any evidence for $^{16}F_{IAS}$ in the $1p$ channel.

4. *γ decay*

The only other energy-allowed, isospin-conserving decay mode for $^{16}F_{IAS}$ is γ decay to a low-lying state in ^{16}F which will then $1p$ decay to $^{15}O_{g.s.}$. The low-lying structure of ^{16}F can be seen in the inset of Fig. 11. While γ decay is normally not competitive with proton decay, for this $\sim$10 MeV $E1$ transition $(0^+ \rightarrow 1^-)$ the estimated (Weisskopf) γ decay lifetime is 2×10^{-18} s (neglecting a possible retardation). This may mean the γ decay lifetime is comparable with forbidden particle decays. We see excess yield of 511 keV γ's in coincidence with $p + {}^{15}O$ events, but our detector was not configured to measure the full energy of such high-energy γ rays. This remains a possible decay channel for $^{16}F_{IAS}$.

G. ^{17}Ne

We are also able to populate two-proton decaying excited states in ^{17}Ne through inelastic excitation of the ^{17}Ne beam. The continuum states of ^{17}Ne up to $E^* = 6.5$ MeV were studied almost 20 years ago through the $^{20}Ne(^{3}He,^{6}He)^{17}Ne$ reaction [29]. In that work, energies, spins, and parities for a large number of excited states were extracted, but no information was obtained about their decays. Here we reexamine the $J^\pi = 5/2^-$ second-excited state in ^{17}Ne.

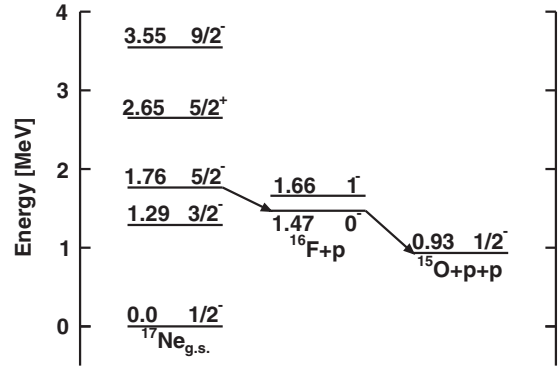

FIG. 13. Partial level scheme for the $2p$ decay of ^{17}Ne. States are labeled by their spin, parity, and energy relative to the ground state of ^{17}Ne.

Figure 13 shows a partial level scheme for ^{17}Ne. While the $3/2^-$ first-excited state is above the $2p$ threshold, it has been shown to decay exclusively by γ-ray emission to the ground state through the nonobservation of the $2p$ decay [30]. That same work measured the $2p$ decay branch of the $5/2^-$ state, and concluded that based on the lifetimes from a simple barrier penetration calculation all of the strength had to go through the 0^- ($\tau = 1.4$ fs) intermediate state and not the 1^- ($\tau = 300$ ps) state. This observation is reasonable given the decay energy to the 1^- state is only 100 keV and the angular momentum in both possible decays is $\ell = 2$. From the momentum correlations in the Jacobi Y coordinate system (see Refs. [1,31]), we can distinguish between these two possible decay paths.

The invariant-mass spectrum for ^{17}Ne in Fig. 14 shows three peaks corresponding to $E^* = 1.764(12)$, 2.651(12), and 3.548(20) MeV states with $J^\pi = 5/2^-$, $5/2^+$ and $9/2^-$ respectively, all seen in [29]. No evidence for the 1.908(15) MeV $1/2^+$ state from that work is seen. An R-matrix fit of the $5/2^-$ peak, filtered by detector acceptance and resolution via Monte Carlo simulation, was performed with a simple quadratic form assumed for the background contribution. The extracted excitation energy is $E^* = 1.77(2)$ MeV which is consistent

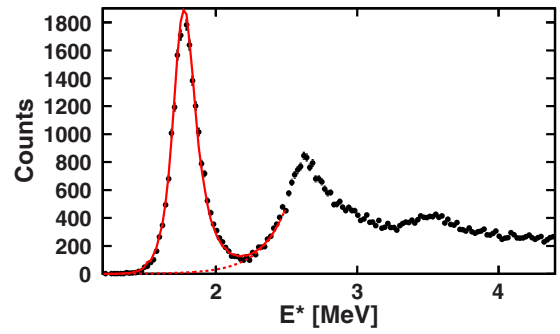

FIG. 14. Excitation-energy spectrum of ^{17}Ne from all detected $2p + {}^{15}O$ events. The solid red curve is an R-matrix fit to the 1.7 MeV $(J^\pi = 5/2^-)$ second-excited state of ^{17}Ne with a quadratic background (red dashed line). Peaks corresponding to the $J^\pi = 5/2^+$ and $9/2^-$ states are seen at higher energy.

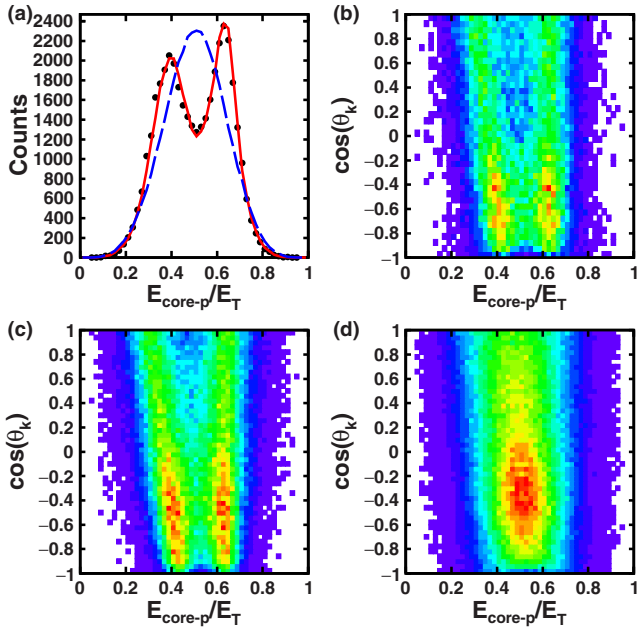

FIG. 15. (a) Jacobi Y energy variable for the $2p$ decay of ^{17}Ne second-excited state. Red solid (blue dashed) curves are Monte Carlo simulations for the decay through the ground state (first-excited state) of the ^{16}F intermediate. (b) Jacobi Y energy-angular correlations for ^{17}Ne second-excited state. The energy variable ($E_{\text{core-p}}/E_T$) is the relative energy between one of the protons and the core, scaled by the total decay energy, and the angular variable (θ_k) is the angle the second proton makes with the center of mass of the core-proton subsystem. (c) and (d) are Monte Carlo predictions for the decay through the ground and first-excited states of ^{16}F respectively.

with the result from the transfer study of Ref. [29]. The lifetime of this state predicted from [30] is $\tau = 1.4$ fs, which corresponds to an intrinsic width of 0.23 eV, far smaller than our detector resolution. Indeed the R-matrix fit of this state is consistent with zero width and thus the lifetime quoted above.

To study the sequential decay in more detail we can make use of the Jacobi Y coordinate system, described in Ref. [31]. The energy variable is the relative energy between the core and one of the protons ($E_{\text{core-p}}/E_T$). The second variable (θ_k) is the angle the other proton makes with the center of mass of the core-proton subsystem. The expected signature of a sequential decay is a double-peaked spectrum in the energy distribution, with one peak corresponding to the decay energy in each step. Figure 15(a) shows the Jacobi Y energy distribution for the $2p$ decay of this state. It has two peaks, one at $\sim$0.35 and one at $\sim$0.65, which is roughly consistent with the decay through the 0^- intermediate state. The energy-angular correlations [Fig. 15(b)] in the Jacobi Y system for this decay exhibit the double-ridge feature seen for sequential decay. Two R-matrix simulations were performed for the decay either through the 0^- or the 1^- intermediate states, with the energy-angular correlation spectra in Figs. 15(c) and 15(d) respectively. Their one-dimensional energy projections are plotted as the red solid and blue dashed curves in Fig. 15(a). The $E_{\text{core-p}}/E_T$ distribution is consistent with the simulation through the 0^-, which confirms the inference of [30].

The outcome of the simulation of the decay through the 1^- is somewhat surprising. In that case the decay energies of the two steps are 100 and 730 keV, with $\Gamma < 40$ keV for the 1^- state [6]. The naïve expectation would be for there to be two peaks at the fractional energies of approximately 0.12 and 0.88; however, only a single peak at 0.5 is seen. To understand why this is the case, one needs to examine the R-matrix line shape input into the Monte Carlo simulation. For the 0^- intermediate state, the peak of the resonance falls in an energy region where the barrier penetration factor changes slowly, and therefore the line shape in the resonance region is not significantly altered. However for the 1^- state, the resonance is in a region where the barrier penetration factor is changing by many orders of magnitude. The result is the peak of the resonance is highly suppressed relative to the tail, and the decay proceeds mainly through the long tail of the resonance line shape. This feature is common for near-threshold decays, and is often referred to as the "ghost peak" [32]. The exact shape depends on the assumed width of the 1^- state; in this case the value of $\Gamma = 40$ keV was taken. However, no choice of Γ for the 1^- intermediate state could reproduce the data.

IV. CONCLUSION

The unbound nucleus, ^{17}Na was observed for the first time. An upper limit on the mass excess was found to be $\Delta M \leqslant 34.72(6)$ MeV. While this is the first experimental identification of any state in ^{17}Na, due to the fact that we do not know if the prominent spectral feature corresponds to the ground state, an excited state, or some mixture of states, only one of the many model predictions can be excluded.

Information on both previously known and unknown excited states in ^{8}B, ^{9}B, and ^{9}C has been presented. For example, in ^{9}C a new width of the lowest $J^\pi = 1/2^-$ state and a candidate for a low-lying positive-parity state, most likely $1/2^+$, are presented.

While we expected the isobaric analog state in ^{16}F to be produced, no clear evidence for this state or the expected decay mode (by direct $2p$ decay to the isobaric analog state in ^{14}N) was observed. This result is consistent with the valence nucleons in the $A = 16$, $T = 2$ states being largely d wave in character, requiring $\ell = 2$ emission for isospin conserving two-nucleon emission. Finally the sequential decay of the second-excited state of ^{17}Ne was measured with high resolution and high statistics and found to decay entirely through the $J^\pi = 0^-$ ground state of ^{16}F.

ACKNOWLEDGMENTS

This work was supported by the U.S. Department of Energy, Division of Nuclear Physics under Grants No. DE-FG02-87ER-40316, No. DE-FG02-04ER-41320, and No. DE-SC0014552 and by the National Science Foundation under Grant No. PHY-0606007. K.W.B. is supported by a National Science Foundation Graduate Research Fellowship under Grant No. DGE-1143954. J.M. is supported by a Department of Energy National Nuclear Security Administration Stewardship Science Graduate Fellowship under cooperative Agreement Number DE-NA0002135.

[1] K. W. Brown, R. J. Charity, L. G. Sobotka, Z. Chajecki, L. V. Grigorenko, I. A. Egorova, Y. L. Parfenova, M. V. Zhukov, S. Bedoor, W. W. Buhro, J. M. Elson, W. G. Lynch, J. Manfredi, D. G. McNeel, W. Reviol, R. Shane, R. H. Showalter, M. B. Tsang, J. R. Winkelbauer, and A. H. Wuosmaa, Phys. Rev. Lett. **113**, 232501 (2014).

[2] K. W. Brown, R. J. Charity, L. G. Sobotka, L. V. Grigorenko, T. A. Golubkova, S. Bedoor, W. W. Buhro, Z. Chajecki, J. M. Elson, W. G. Lynch, J. Manfredi, D. G. McNeel, W. Reviol, R. Shane, R. H. Showalter, M. B. Tsang, J. R. Winkelbauer, and A. H. Wuosmaa, Phys. Rev. C **92**, 034329 (2015).

[3] K. W. Brown, W. W. Buhro, R. J. Charity, J. M. Elson, W. Reviol, L. G. Sobotka, Z. Chajecki, W. G. Lynch, J. Manfredi, R. Shane, R. H. Showalter, M. B. Tsang, D. Weisshaar, J. R. Winkelbauer, S. Bedoor, and A. H. Wuosmaa, Phys. Rev. C **90**, 027304 (2014).

[4] M. Wallace, M. Famiano, M.-J. van Goethem, A. Rogers, W. Lynch, J. Clifford, F. Delaunay, J. Lee, S. Labostov, M. Mocko, L. Morris, A. Moroni, B. Nett, D. Oostdyk, R. Krishnasamy, M. Tsang, R. de Souza, S. Hudan, L. Sobotka, R. Charity, J. Elson, and G. Engel, Nucl. Instrum. Methods Phys. Res., Sect. A **583**, 302 (2007).

[5] D. Weisshaar, A. Gade, T. Glasmacher, G. Grinyer, D. Bazin, P. Adrich, T. Baugher, J. Cook, C. Diget, S. McDaniel, A. Ratkiewicz, K. Siwek, and K. Walsh, Nucl. Instrum. Methods Phys. Res., Sect. A **624**, 615 (2010).

[6] Evaluated Nuclear Structure Data File (ENSDF), http://www.nndc.bnl.gov/ensdf/

[7] K. Amos, L. Canton, P. Fraser, S. Karataglidis, J. Svenne, and D. van der Knijff, Nucl. Phys. A **879**, 132 (2012).

[8] N. K. Timofeyuk and P. Descouvemont, Phys. Rev. C **81**, 051301 (2010).

[9] H. T. Fortune and R. Sherr, Phys. Rev. C **82**, 027310 (2010).

[10] H. T. Fortune, Phys. Rev. C **90**, 067302 (2014).

[11] P. R. Fraser, L. Canton, K. Amos, S. Karataglidis, J. P. Svenne, and D. van der Kniff, in Proceedings of the International Conference on Nuclear Reaction Mechanism, 2013 (unpublished), p. 271.

[12] J. Tian, N. Wang, C. Li, and J. Li, Phys. Rev. C **87**, 014313 (2013).

[13] Z. Elekes, Z. Dombrádi, R. Kanungo, H. Baba, Z. Fülöp, J. Gibelin, Á. Horváth, E. Ideguchi, Y. Ichikawa, N. Iwasa, H. Iwasaki, S. Kanno, S. Kawai, Y. Kondo, T. Motobayashi, M. Notani, T. Ohnishi, A. Ozawa, H. Sakurai, S. Shimoura, E. Takeshita, S. Takeuchi, I. Tanihata, Y. Togano, C. Wu, Y. Yamaguchi, Y. Yanagisawa, A. Yoshida, and K. Yoshida, Phys. Lett. B **614**, 174 (2005).

[14] H. G. Bohlen, R. Kalpakchieva, W. von Oertzen, T. N. Massey, A. A. Ogloblin, G. de Angelis, M. Milin, C. Schulz, T. Kokalova, and C. Wheldon, Eur. Phys. J. A **31**, 279 (2007).

[15] A. M. Lane and R. G. Thomas, Rev. Mod. Phys. **30**, 257 (1958).

[16] W. Benenson and E. Kashy, Phys. Rev. C **10**, 2633 (1974).

[17] K. M. Nollett, Phys. Rev. C **86**, 044330 (2012).

[18] N. K. Timofeyuk, Phys. Rev. C **92**, 034330 (2015).

[19] M. S. Golovkov, V. Z. Goldberg, L. S. Danelyan, V. I. Dukhanov, I. L. Kuleshov, A. E. Pakhomov, I. N. Serikov, V. A. Timofeev, and V. N. Unezhev, Yad. Fiz. **53**, 888 (1991) [Sov. J. Nucl. Phys. **54**, 719 (1991)].

[20] R. J. Charity, J. M. Elson, J. Manfredi, R. Shane, L. G. Sobotka, B. A. Brown, Z. Chajecki, D. Coupland, H. Iwasaki, M. Kilburn, J. Lee, W. G. Lynch, A. Sanetullaev, M. B. Tsang, J. Winkelbauer, M. Youngs, S. T. Marley, D. V. Shetty, A. H. Wuosmaa, T. K. Ghosh, and M. E. Howard, Phys. Rev. C **84**, 014320 (2011).

[21] M. Wang, G. Audi, A. Wapstra, F. Kondev, M. MacCormick, X. Xu, and B. Pfeiffer, Chin. Phys. C **36**, 1603 (2012).

[22] N. Auerbach, Phys. Rep. **98**, 273 (1983).

[23] Y. Utsuno, Phys. Rev. C **70**, 011303 (2004).

[24] B. A. Brown, A. Etchegoyen, N. S. Godwin, W. D. M. Rae, W. A. Richter, W. E. Ormand, E. K. Warburton, J. S. Winfield, L. Zhao, and C. H. Zimmerman, MSU-NSCL (Michigan State University, National Superconducting Cyclotron Laboratory) Technical Report No. 1289, 2004 (unpublished).

[25] E. K. Warburton and B. A. Brown, Phys. Rev. C **46**, 923 (1992).

[26] J. P. Mitchell, G. V. Rogachev, E. D. Johnson, L. T. Baby, K. W. Kemper, A. M. Moro, P. Peplowski, A. S. Volya, and I. Wiedenhöver, Phys. Rev. C **87**, 054617 (2013).

[27] M. F. Jager, R. J. Charity, J. M. Elson, J. Manfredi, M. H. Mahzoon, L. G. Sobotka, M. McCleskey, R. G. Pizzone, B. T. Roeder, A. Spiridon, E. Simmons, L. Trache, and M. Kurokawa, Phys. Rev. C **86**, 011304 (2012).

[28] R. J. Charity, J. M. Elson, J. Manfredi, R. Shane, L. G. Sobotka, Z. Chajecki, D. Coupland, H. Iwasaki, M. Kilburn, J. Lee, W. G. Lynch, A. Sanetullaev, M. B. Tsang, J. Winkelbauer, M. Youngs, S. T. Marley, D. V. Shetty, A. H. Wuosmaa, T. K. Ghosh, and M. E. Howard, Phys. Rev. C **84**, 051308 (2011).

[29] V. Guimarães, S. Kubono, N. Ikeda, I. Katayama, T. Nomura, M. H. Tanaka, Y. Fuchi, H. Kawashima, S. Kato, H. Toyokawa, C. C. Yun, T. Niizeki, T. Kubo, M. Ohura, and M. Hosaka, Phys. Rev. C **58**, 116 (1998).

[30] M. J. Chromik, P. G. Thirolf, M. Thoennessen, B. A. Brown, T. Davinson, D. Gassmann, P. Heckman, J. Prisciandaro, P. Reiter, E. Tryggestad, and P. J. Woods, Phys. Rev. C **66**, 024313 (2002).

[31] I. A. Egorova, R. J. Charity, L. V. Grigorenko, Z. Chajecki, D. Coupland, J. M. Elson, T. K. Ghosh, M. E. Howard, H. Iwasaki, M. Kilburn, J. Lee, W. G. Lynch, J. Manfredi, S. T. Marley, A. Sanetullaev, R. Shane, D. V. Shetty, L. G. Sobotka, M. B. Tsang, J. Winkelbauer, A. H. Wuosmaa, M. Youngs, and M. V. Zhukov, Phys. Rev. Lett. **109**, 202502 (2012).

[32] F. C. Barker, G. M. Crawley, P. S. Miller, and W. F. Steele, Aust. J. Phys. **29**, 245 (1976).